Journal of Catalysis 268 (2009) 1–8

Contents lists available at ScienceDirect

Journal of Catalysis

journal homepage: www.elsevier.com/locate/jcat

Catalytic performance and characterization of Rh–CeO_2/MgO catalysts for the catalytic partial oxidation of methane at short contact time

Hisanori Tanaka [a], Rie Kaino [a], Kazu Okumura [b], Tokushi Kizuka [a], Keiichi Tomishige [a,c,*]

[a] Graduate School of Pure and Applied Sciences, University of Tsukuba, 1-1-1, Tennodai, Tsukuba, Ibaraki 305-8573, Japan
[b] Department of Chemistry and Biotechnology, Graduate School of Engineering, Tottori University, Koyama-cho Minami, Tottori 680-8552, Japan
[c] Japan Science and Technology Agency, CREST, 1-1-1, Tennodai, Tsukuba, Ibaraki 305-8573, Japan

ARTICLE INFO

Article history:
Received 20 June 2009
Revised 18 August 2009
Accepted 19 August 2009
Available online 27 September 2009

Keywords:
Catalytic partial oxidation
Methane
Thermography
Hot spot
Rhodium
Ceria

ABSTRACT

The addition of an optimum amount of CeO_2 (Ce/Rh = 4) to 1.0 wt% Rh/MgO promoted the catalytic partial oxidation (CPO) of methane with N_2 dilution. At the same time, it can suppress the temperature increase at the catalyst bed inlet during the CPO of methane without N_2 dilution. The Rh–CeO_2/MgO (Ce/Rh = 4) has the ability to maintain a more reduced state in the CPO of methane, and this may be related to the high ability to activate methane by the synergy of Rh metal surface and partially covering Ce species. The catalyst bed of the CPO of methane consists of the initial oxidation zone and the subsequent steam reforming zone. The catalyst with higher resistance to the oxidation of Rh gives larger zone for the steam reforming and it also enables the overlap of the exothermic oxidation zone with the endothermic steam reforming zone.

1. Introduction

Conversion of natural gas to synthesis gas is important for the production of methanol, dimethyl ether, and Fischer–Tropsch liquids, and a more compact and energy-efficient process for syngas production than conventional steam reforming is needed [1,2]. Much attention has recently been paid to the catalytic partial oxidation (CPO) of methane, where high methane conversion and syngas yield have been obtained at millisecond contact times under autothermal conditions [3]. Therefore, CPO makes the reactors simple and compact and it also enables fast responses and low heat capacity. It has been confirmed that noble-metal-based catalysts are highly active for the CPO of methane, and Rh is one of the suitable components [3–7]. It has been known that rhodium is applied to various catalytic reactions other than partial oxidation of methane, and modification of Rh catalysts with CeO_2 promoted many reactions such as deNOx [8,9], CO oxidation [10], reforming of hydrocarbons [11,12], gasification of biomass [13–15], catalytic partial oxidation and autothermal reforming of ethanol [16,17], and catalytic wet air oxidation of gasoline oxygenates [18]. In the CPO of methane, Schmidt and co-workers have reported that the effect of the washcoat and Ce addition was investigated over Rh + CeO_2-based catalysts supported on α-Al_2O_3 foam monoliths using the spatial analysis of gas composition and temperature profiles in the catalyst bed [19–21]. In the present study, the effect of CeO_2 addition to Rh/MgO is investigated in the CPO of methane at short contact time. In the case of the practical application of the CPO of methane, the reaction pressure will be higher such as 1 MPa, although the CPO performance has been evaluated under atmospheric pressure or below. Under pressurized conditions, the suppression of carbon deposition will be more important. MgO is known to be an effective support to the suppression of carbon deposition in the production of synthesis gas by the reforming reactions [22,23]. The addition of CeO_2 to MgO decreased the amount of carbon deposition in the CPO of methane under pressurized condition [24]. In addition, it has been reported that the MgO support suppressed the sintering of Rh metal particles [25–27].

In this article, we investigated the dependence of the added amount of CeO_2 over 1 wt% Rh/MgO on the CPO of methane with or without dilution. In particular, the effect of CeO_2 addition on the catalyst structure and the reaction zones of CPO are discussed on the basis of the catalyst bed temperature measured by the infrared thermographical observation and catalyst characterization results.

2. Experimental

2.1. Catalyst preparation

A Rh/MgO catalyst was prepared by impregnating MgO with an aqueous solution of $RhCl_3 \cdot 3H_2O$ (Soekawa Chemicals). The MgO

* Corresponding author. Address: Graduate School of Pure and Applied Sciences, University of Tsukuba, 1-1-1, Tennodai, Tsukuba, Ibaraki 305-8573, Japan. Fax: +81 29 853 5030.
E-mail address: tomi@tulip.sannet.ne.jp (K. Tomishige).

0021-9517/$ - see front matter © 2009 Elsevier Inc. All rights reserved.
doi:10.1016/j.jcat.2009.08.008

support was prepared by calcining MgO (UBE Material Industries Ltd., Japan) at 1423 K for 3 h. After the impregnation, the solvent was evaporated at 353 K and the sample was dried at 383 K for 12 h and then calcined at 773 K in air for 3 h. Rh–CeO_2/MgO catalysts were prepared by impregnating MgO with the mixed aqueous solution of $RhCl_3{\cdot}3H_2O$ and $Ce(NH_4)_2(NO_3)_6{\cdot}H_2O$ (Wako Pure Chemical Industries) in the co-impregnation method. After the co-impregnation, the solvent was evaporated at 353 K. The sample was dried at 383 K for 12 h and then calcined at 773 K for 3 h. The loading amount of Rh on Rh/MgO and Rh–CeO_2/MgO was 1.0 wt%. The loading amounts of CeO_2 on Rh–CeO_2/MgO were represented as the molar ratio of Ce to Rh (Ce/Rh) in parentheses as Rh–CeO_2/MgO (Ce/Rh = 4). The weight content of the CeO_2 is listed out in Table 1. As a reference, CeO_2/MgO was also prepared by the impregnation method. The loading amount of CeO_2 was adjusted to the corresponding Rh–CeO_2/MgO. Catalysts in powder form were pressed, then crushed and sieved into granules of 0.13–0.18 mm.

2.2. Characterization of catalysts

Temperature-programed reduction (TPR) profiles were measured in a fixed-bed quartz reactor, and the procedures were the same as those mentioned in the previous report [28]. Before TPR measurement, the catalysts were treated in O_2 at 773 K for 0.5 h and then in Ar at 773 K for 0.5 h to remove adsorbed species such as CO_2. The sample weight was 50 mg, and the heating rate was 10 K min^{-1} from room temperature to 1123 K, and 5% H_2 diluted in Ar (30 cm^3 min^{-1}) was used. Consumption of hydrogen was estimated from the integrated peak area of the profiles.

Measurement of H_2 chemisorption was carried out in a high-vacuum system using a volumetric method, and the procedures were the same as those mentioned in the previous report [28]. Before the adsorption of H_2, the catalysts were treated in H_2 at 1123 K for 0.5 h in a fixed-bed reactor. After this pretreatment, the sample was transferred to a cell for adsorption measurements under air atmosphere. Before each measurement, H_2 pretreatment at 773 K was carried out for 0.5 h in the cell. After evacuation at 773 K, the sample was cooled to room temperature. The total amount of H_2 adsorption was measured at room temperature with a H_2 pressure at adsorption equilibrium of about 1.0 kPa. The dead volume of the apparatus was 63.5 cm^3 and the sample weight was 150 mg.

The catalysts were observed using a transmission electron microscope (TEM) (JEOL JEM-2010) at an accelerating voltage of 200 kV. Catalysts after the H_2 reduction pretreatment at 1123 K for 0.5 h and after the activity test were dispersed in ethanol using supersonic waves. Then they were put on Cu grids for TEM observation under air atmosphere. Average particle size in the form of a surface mean diameter (d_s) is calculated by $d_s = \sum n_1 d_1^3 / \sum n_1 d_1^2$ (n_i, number of pieces; d_i, particle size) [29–31].

Rh *K*-edge EXAFS were measured at BL01B1 station in SPring-8 with support from the Japan Synchrotron Radiation Research Institute (JASRI) (Proposal Nos. 2006A1058, 2007A1156), and the measurement method and the beam conditions were the same as those reported previously [28]. The catalyst powder (750 mg) was treated using H_2 at 1123 K for 0.5 h in a fixed-bed reactor and the sample was pressed into a self-supporting 7-mm-diameter wafer under atmosphere, followed by treatment with H_2 at 773 K for 0.5 h in a cell. After this pretreatment, the sample wafer was transferred to the measurement cell using a glove box filled with nitrogen to prevent exposure of the sample disk to air. The analysis method for the EXAFS spectra was carried out in the same way as that in the previous report [28].

2.3. Partial oxidation of methane with or without N_2 dilution

Activity tests for the catalytic partial oxidation (CPO) of methane with N_2 dilution were carried out using a tubular fixed bed flow reactor made of quartz. The reactor setup was the same as that in the previous report [28]. The dilution of the reactant gases with N_2 ($CH_4/O_2/N_2$ = 4/2/94) was applied to suppress the temperature increase of the catalyst bed due to exothermic reactions. The catalyst weight was 10 mg, and the height of the catalyst bed was about 1.4 mm. Catalysts were reduced with hydrogen at 1123 K for 0.5 h before each activity test. The temperature on the reactor was monitored with a thermocouple at the bottom of the catalyst bed, and it was denoted as T_{TC}. The total flow rate of the gases was 1500 cm^3 min^{-1}, and the contact time was as short as 0.4 ms. The temperature profile of the catalyst bed during the CPO of methane with the N_2 dilution was measured by using the infrared thermography, and the profile is shown in Fig. S1. The bed temperature was only 20 K higher than the T_{TC}, indicating that the effect of the temperature increase in the CPO of methane with N_2 dilution is

Table 1
Properties of catalysts and results of activity test in partial oxidation of methane with N_2 dilution.

Catalyst	Loading of CeO_2 (wt%)	BET surface area (m^2 g^{-1})	H_2 adsorption (μmol g_{cat}^{-1})[a]	Rh metal particle size (nm)[b]	Dispersion		Partial oxidation of methane[c]			
					H_2 adsorption (H/Rh)	TEM[d]	CH_4 conversion (%)	H_2 selectivity (%)	CO selectivity (%)	TOF (s^{-1})[e]
Rh/MgO	–	6.9	11.2	5.6 ± 0.3	0.24	0.20	69	83	81	125
Rh–CeO_2/MgO (Ce/Rh = 4)	6.4	9.8	6.0	4.1 ± 0.3	0.13	0.27	81	93	90	274
Rh–CeO_2/MgO (Ce/Rh = 8)	12.8	11.5	4.8	–	0.10	–	72	88	84	303
Rh–CeO_2/MgO (Ce/Rh = 12)	19.2	12.8	4.0	–	0.09	–	70	87	84	352
Rh–CeO_2/MgO (Ce/Rh = 18.7)	30.0	15.0	4.0	3.2 ± 0.3	0.09	0.34	64	87	80	323
6.4 wt% CeO_2/MgO[f]	6.4	10.2	–	–	–	–	0.3	28	12	–
30 wt% CeO_2/MgO[f]	30.0	14.6	–	–	–	–	0.5	36	9	–

[a] H_2 adsorption at 298 K.
[b] Rh particle size (surface-averaged) is calculated from TEM images.
[c] Reaction conditions: $CH_4/O_2/N_2$ = 4/2/94, total flow rate 1500 cm^3 min^{-1}; T_{TC} = 973 K; total pressure 0.1 MPa; catalyst weight 10 mg; contact time 0.4 ms.
[d] Dispersion from TEM is calculated from (1.098/(Rh particle size [nm])) [34].
[e] Turnover frequency (TOF) in partial oxidation of methane is calculated on the basis of methane conversion rate and the amount of H_2 adsorption at 298 K.
[f] Loading amounts of CeO_2 on 6.4 and 30 wt% CeO_2/MgO were equal to those on Rh–CeO_2/MgO (Ce/Rh = 4 and 18.7), respectively.

much smaller than that in without N_2 dilution, and this can be regarded as isothermal conditions.

Reaction tests for partial oxidation of methane ($CH_4/O_2 = 2/1$) without N_2 dilution were also carried out using a fixed-bed quartz reactor. The reactor setup was the same as that reported previously [28]. In the case of the CPO of methane without the dilution, the catalyst temperature during the reaction was measured by the infrared thermography (TH31; NEC San-ei Instruments Ltd.), as reported in the previous reports [28,32,33]. The apparatus detected the infrared with 3.2 μm wavelength and the temperature resolution was ±5 K, and the spatial resolution was 0.8 mm. The calibration was done on the basis of the catalyst bed temperature with the flow of an inert gas (N_2) and heating only by the furnace, whose temperature was controlled by the thermocouple. The calibration includes the emission coefficient of the catalysts. The temperature profiles of catalyst bed were measured from a window (15 mm × 15 mm) on furnace. The furnace temperature was controlled at 723 K. The total flow rate was 300 $cm^3\ min^{-1}$, the catalyst weight was 10 mg, the height of the catalyst bed was 3 mm, and the contact time was 2.0 ms.

In both reaction tests of the CPO with and without N_2 dilution, the catalysts were reduced with hydrogen at 1123 K for 0.5 h before each activity test. The contact time in the experimental result is represented on the basis of the density of Rh–CeO_2/MgO (Ce/Rh = 4), since a density of catalysts increased 20% monotonously from Rh/MgO to Rh–CeO_2/MgO (Ce/Rh = 18.7), and the contact time is also changed when the catalyst weight is fixed. The effluent gas was analyzed using an FID-GC equipped with a methanator for CO, CH_4, and CO_2, a TCD-GC (carrier gas: Ar) for H_2 and a TCD-GC (carrier gas: He) for O_2. The on-line sampling of the six-way valves was used. Methane conversion and CO and H_2 selectivities are calculated as

$$\text{CH}_4\ \text{conversion}\ (\%) = (C_{\text{CO}} + C_{\text{CO}_2})/(C_{\text{CH}_4} + C_{\text{CO}} + C_{\text{CO}_2}) \times 100,$$
$$\text{CO selectivity}\ (\%) = C_{\text{CO}}/(C_{\text{CO}} + C_{\text{CO}_2}) \times 100,$$
$$\text{H}_2\ \text{selectivity}\ (\%) = C_{\text{H}_2}/((C_{\text{CO}} + C_{\text{CO}_2}) \times 2) \times 100,$$

where C is the concentration of each component in the effluent gases. Throughout the experiments, no carbon-containing product other than CO and CO_2 was formed. Amount of deposited carbon was negligible based on the thermogravimetric analysis (TGA) of the catalysts after the reaction. An example of the TGA profile is shown in Fig. S2, and no weight decrease with an exothermic behavior due to the carbon combustion was observed at all.

2.4. Titration of adsorbed oxygen during the partial oxidation of methane

To examine the oxidation degree of catalysts during partial oxidation of methane, titration of adsorbed/absorbed oxygen with H_2 pulses was carried out after the pulse reaction of partial oxidation of methane. The reactor setup was the same as that for the CPO without the dilution. Pulse gases were supplied to the reactor using six-way valves and He carrier gas. The catalyst amount was 10 mg, which contained 0.93 μmol Rh. After H_2 pretreatment at 1123 K for 0.5 h, 10 pulses of $CH_4 + O_2$ were introduced at 873 K. The single pulse for the partial oxidation of methane contained 4.0 μmol CH_4 + 2.0 μmol O_2 with He carrier gas at 300 $cm^3\ min^{-1}$, and the amount was much larger than total Rh amount and the number of surface Rh atoms, indicating that the large turnover number can be obtained. After the pulse reaction, the reactor was purged with He rapidly, and then the H_2 pulse (0.46 μmol) was supplied repeatedly at 1123 K, which was the same temperature as that in the reduction pretreatment. The total consumption of H_2 pulses corresponds to the oxidation during the pulse CPO of methane. Reactants and products were analyzed using a quadrupole mass spectrometer (QMS, QMA200; Pfeiffer Vacuum Technology AG). Stable catalytic performance in CH_4 conversion, H_2 selectivity, and CO selectivity during 10 pulses of the CPO of methane suggests that the result of the pulse experiment can be reflected by that of the steady-state condition.

2.5. Ability of the catalysts to activate methane with or without preadsorbed oxygen

To evaluate the ability of the catalysts to activate methane, the reactivity of CH_4 was measured by the CH_4 pulse reaction. In addition, the reactivity was also compared between reduced and oxygen-pretreated catalysts because the catalyst bed in the CPO of methane has two zones: oxidation zone and the reforming zone [19]. Catalysts without preadsorbed oxygen were reduced catalysts with hydrogen at 1123 K for 0.5 h. On the other hand, the O_2 pulse (0.45 μmol) was supplied at 373 K to the reduced catalysts repeatedly and the amount of adsorbed and absorbed oxygen was adjusted on the basis of the QMS analysis during the O_2 pulse feeding. The O_2 treatment temperature was set to as low as 373 K because O_2 molecule can be trapped by the absorption into Rh near the catalyst bed inlet at high temperature. After purging the reactor with He, the CH_4 pulse (1.2 μmol with He carrier gas at 100 $cm^3\ min^{-1}$) at 773 K was supplied to 0.1 g catalyst containing 9.3 μmol Rh. The temperature of the methane pulse reaction was lower than the CPO experiments to keep the amount of the converted methane smaller than that of the surface Rh. At this temperature, the methane conversion can reflect the probability of methane activation of surface Rh. At high temperature, catalytic methane decomposition to solid carbon and H_2 can proceed and methane conversion is too high to evaluate the probability of methane activity. In this experiment, only hydrogen was observed as a product, and the formation of CO and CO_2 was below the detection limit of the QMS analysis.

3. Results and discussion

3.1. Characterization of Rh–CeO_2/MgO catalysts

Fig. 1 shows TEM images of Rh/MgO, Rh–CeO_2/MgO (Ce/Rh = 4 and 18.7), and CeO_2/MgO catalysts after the H_2 reduction pretreatment. Small spherical dark spots were observed on three Rh-containing catalysts (Fig. 1a–c), and they are not observed on CeO_2/MgO (Fig. 1d), therefore, these spots are assigned to Rh metal particles. The average Rh particle sizes (surface-averaged) were determined from the TEM observation and the dispersions calculated from them are summarized in Table 1 [34]. The Rh dispersions estimated by H_2 chemisorption are also shown in Table 1. In the case of Rh–CeO_2/MgO catalysts, it is found that the dispersion (H/Rh) obtained from H_2 adsorption is much smaller than that estimated by TEM result, and it is suggested that the surface of Rh metal particles can be partially covered with Ce species. This kind of structure agreed well with the previous reports on Rh + CeO_2-based catalysts [35–37]. It should be noted that Rh metal particle size decreased gradually with increasing CeO_2 amount.

The structure of Rh was characterized by Rh *K*-edge EXAFS. The EXAFS spectra are shown in Fig. S3. Curve fitting results of Rh *K*-edge EXAFS after H_2 reduction are presented in Table 2, where a good fitting was attained using only the Rh–Rh bond. Intensities of the peak due to the Rh–Rh bond in the Fourier transform spectra (Fig. S3b) decreased gradually with increasing CeO_2 amount. At the same time, the coordination number (CN) of the Rh–Rh bond decreased with increasing CeO_2 amount. Even in the case of Rh–CeO_2/MgO (Ce/Rh = 18.7) with smaller Rh particles, other bonds like Rh–O than Rh–Rh cannot be detected. The dependence of the

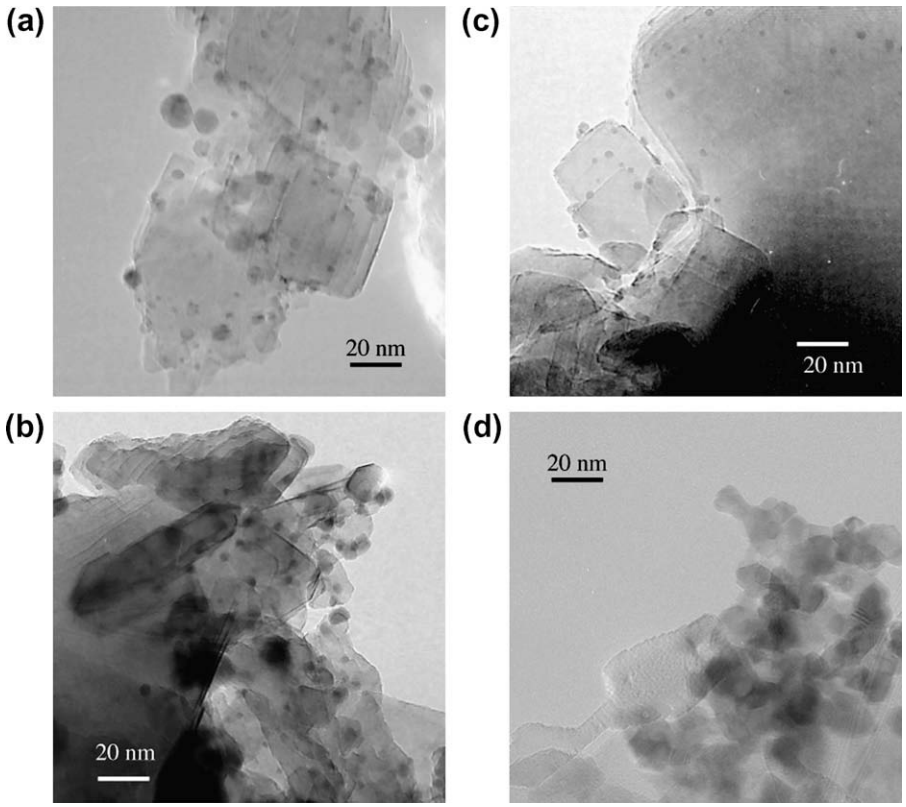

Fig. 1. TEM images of Rh/MgO (a), Rh–CeO_2/MgO (Ce/Rh = 4 (b) and 18.7 (c)), and 6.4 wt% CeO_2/MgO (d) catalysts after H_2 reduction at 1123 K.

Ce/Rh ratio on the CN of the Rh–Rh bond can be explained by the decrease of Rh metal particle size caused by CeO_2 addition, and this behavior is supported by TEM results.

Fig. 2 shows TPR profiles of the catalysts with H_2, and Table 3 lists out H_2 consumption data. Reduction of Rh species on MgO proceeds mainly at 400–800 K [25–27]. According to the previous reports, H_2 consumption below 673 K was assigned to the reduction of Rh_2O_3, and H_2 consumption above 673 K was assigned to the reduction of $MgRh_2O_4$ [25–27]. As listed out in Table 3, the total amount of H_2 consumption on Rh/MgO was explained by the stoichiometry of the reduction of Rh^{3+} to Rh^0 in Rh_2O_3 and $MgRh_2O_4$ ($Rh^{3+} + 3/2H_2 \rightarrow 2Rh^0 + 3H^+$), indicating that almost all the Rh species are present in a metallic state after the reduction. On CeO_2/MgO, the CeO_2 species on MgO were reduced at around 860 K. For Rh–CeO_2/MgO, a TPR peak at 460 K grew with increasing CeO_2 amount, where the H_2 was consumed by the reduction of both Rh_2O_3 and CeO_2 because the H_2 consumption in the temperature range of r.t. to 600 K was larger than 1.5 times of total Rh mol. In addition, the amount of the reduced CeO_2 on Rh–CeO_2/MgO (Ce/Rh = 8) was larger than that on CeO_2/MgO with the same CeO_2 loading amount. It should be noted that the amount of the reduced Ce species increased with increasing CeO_2 amount, but the ratio of reduced Ce species to the total Ce species decreased with CeO_2 loading. From these results it can be observed that the presence of Rh can promote the reduction of CeO_2 within the region where spilt-over hydrogen can reach [38,39]. In particular, the increase of the peak intensity below 600 K with increasing CeO_2 amount indicates the strong interaction between Rh and CeO_2, and this interaction is connected to the formation of Rh metal particles covered with CeO_2 suggested by the results given in Table 1. Decoration of metal particles with reduced oxide species has been known as SMSI (strong metal–support interaction) and SMOI (strong metal–oxide interaction) phenomena [40,41].

3.2. Catalytic performance in partial oxidation of methane with N_2 dilution

Table 1 shows how the amount of CeO_2 affects methane conversion and selectivity over Rh–CeO_2/MgO and CeO_2/MgO. The conversion and selectivity increased by the addition of CeO_2 at Ce/Rh = 4, but they decreased with increasing CeO_2 amount in the range of Ce/Rh = 4–18.7. As a result, the optimum amount of CeO_2 over Rh/MgO is determined to be Ce/Rh = 4. As a reference, we prepared 6.4 and 30 wt% CeO_2 supported on MgO, whose loading amounts corresponded to that supported on Rh–CeO_2/MgO (Ce/Rh = 4 and 18.7), and it is found that the activity of CeO_2/MgO was very low, and the increase of conversion and selectivity on Rh–CeO_2/MgO (Ce/Rh = 4) cannot be explained by the contribution of CeO_2 itself. In addition, it should be noted that the adsorption amount of H_2 decreased gradually with increasing CeO_2 amount, and this tendency does not agree with the behavior of methane conversion. Reasons for high methane conversion on Rh–CeO_2/MgO (Ce/Rh = 4) are discussed later.

3.3. Catalytic performance in partial oxidation of methane without N_2 dilution

Without the dilution, the catalyst bed temperature is strongly influenced by the catalytic performance, regarding the CPO of methane [28]. Fig. 3 shows the results of thermographical observation during the CPO of methane without N_2 dilution, and the results of the test are summarized in Table 4. The highest bed temperature on Rh–CeO_2/MgO (Ce/Rh = 4) was lower than those on the other catalysts tested, and the bed temperature increased with increasing CeO_2 amounts on the Rh–CeO_2/MgO in the range of Ce/Rh > 4. This tendency in the bed temperature was opposite to the catalytic activity in the CPO of methane with N_2 dilution (Table 1). Generally speaking, it is not easy to distinguish the

Table 2
Curve fitting results of Rh *K*-edge EXAFS of the reduced catalysts.

Catalyst	Shells	CN[a]	R^b (10^{-1} nm)	σ^c (10^{-1} nm)	$\Delta E_0{}^d$ (eV)	$R_f{}^e$ (%)
Rh/MgO	Rh–Rh	10.8 ± 0.8	2.68 ± 0.01	0.068 ± 0.002	0.6 ± 1.9	0.26
Rh–CeO_2/MgO (Ce/Rh = 4)	Rh–Rh	9.6 ± 1.0	2.67 ± 0.01	0.069 ± 0.003	3.1 ± 2.2	0.29
Rh–CeO_2/MgO (Ce/Rh = 8)	Rh–Rh	9.0 ± 0.8	2.67 ± 0.01	0.069 ± 0.003	1.9 ± 2.0	0.27
Rh–CeO_2/MgO (Ce/Rh = 12)	Rh–Rh	8.3 ± 1.0	2.67 ± 0.01	0.069 ± 0.003	−1.8 ± 1.6	0.20
Rh–CeO_2/MgO (Ce/Rh = 18.7)	Rh–Rh	7.6 ± 0.9	2.66 ± 0.01	0.070 ± 0.004	0.5 ± 2.6	0.47
Rh foil	Rh–Rh	12.0	2.68	0.060	0	

[a] Coordination number.
[b] Bond distance.
[c] Debye–Waller factor.
[d] Difference in the origin of photoelectron energy between the reference and the sample.
[e] Residual factor. Fourier transform range: 30–160 nm, Fourier filtering range: 0.153–0.273 nm.

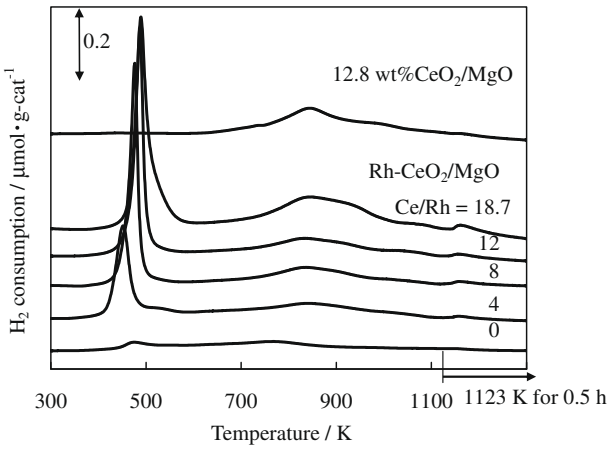

Fig. 2. TPR profiles of Rh–CeO_2/MgO and CeO_2/MgO.

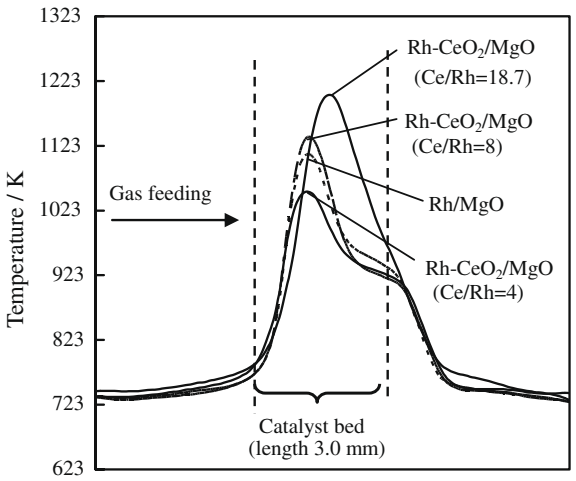

Fig. 3. Result of thermographical observation during the partial oxidation of methane. Reaction conditions: CH_4/O_2 = 2/1, total flow rate 300 cm^3 min^{-1}; total pressure 0.1 MPa; catalyst weight 10 mg; and contact time 2.0 ms. Furnace temperature 723 K.

different reaction zones, such as reforming, partial oxidation, and combustion, only from the thermography as quasi-spatially resolved technique, and it is necessary to analyze the gas composition at each position in the catalyst bed [5,42,43]. Here, the effect of CeO_2 is attempted to be discussed on the basis of the temperature profiles of the catalyst bed. As reported previously, it is thought that the CPO of methane at millisecond contact times consists of an initial oxidation zone in which predominantly CO and H_2O are formed ($CH_4 + 1.5O_2 \rightarrow CO + 2H_2O$, $\Delta H = -519$ kJ/mol, (1)), followed by steam reforming zone ($CH_4 + H_2O \rightarrow CO + 3H_2$, $\Delta H = 210$ kJ/mol, (2)) [44,45]. In the initial oxidation zone, the total oxidation (combustion) of methane ($CH_4 + 2O_2 \rightarrow CO_2 + 2H_2O$, $\Delta H = -802.3$ kJ/mol, (3)) can also proceed as a side reaction. When the oxidation of methane with O_2 such as (1) and (3) proceeds, the catalyst bed temperature was increased by these highly exothermic reactions. On the other hand, since the steam reforming of methane is highly endothermic reaction, the catalyst bed temperature can be decreased in the steam reforming zone. The initial oxidation zone is located near the catalyst bed inlet and this can explain the temperature increase in Fig. 3. The highest temperature is influenced by the selectivity of oxidation to CO or CO_2 and catalytic activity of the oxidation reaction.

Another important point is that the temperature gradients can decrease due to the overlap of the oxidation and the reforming zones [19,46–48]. In order to discuss the contributions of the oxidation, the reforming of methane, and the overlap, we have to get the information of the degree of oxidation of catalyst surface in the

Table 3
Results of temperature-programed reduction.

Catalyst	Ce/Rh	Loading amount (μmol g_{cat}^{-1})		H_2 consumption (μmol g_{cat}^{-1})		Amount of reduced CeO_2 (μmol g_{cat}^{-1})[a]
		Rh	CeO_2	r.t. to 600 K	600–1123 K	r.t. to 1123 K
Rh/MgO	0	93	–	37	98	–
Rh–CeO_2/MgO	4	93	373	150	150	320
	8	93	746	201	158	438
	12	93	1119	218	165	488
	18.7	93	1744	265	243	735
12.8 wt% CeO_2/MgO[b]	–	–	746	11	163	347

[a] Assuming that all the Rh species are reduced ($Rh^{3+} \rightarrow Rh^0$) and stoichiometry of the CeO_2 reduction ($2CeO_2 + H_2 \rightarrow Ce_2O_3 + H_2O$).
[b] Loading amount of CeO_2 on 12.8 wt% CeO_2/MgO was equal to that on Rh–CeO_2/MgO (Ce/Rh = 8).

Table 4
Catalyst performance and bed temperature in partial oxidation of methane without N_2 dilution.

Catalyst	Partial oxidation of methane[a]			Temperature (K)	
	CH_4 conversion (%)	H_2 selectivity (%)	CO selectivity (%)	Highest bed	Outlet
Rh/MgO	78	93	91	1109 ± 5	941 ± 5
Rh–CeO_2/MgO (Ce/Rh = 4)	77	93	90	1052 ± 5	928 ± 5
Rh–CeO_2/MgO (Ce/Rh = 8)	76	87	89	1122 ± 5	922 ± 5
Rh–CeO_2/MgO (Ce/Rh = 12)	76	87	88	1135 ± 5	923 ± 5
Rh–CeO_2/MgO (Ce/Rh = 18.7)	71	87	85	1201 ± 5	994 ± 5

[a] Reaction conditions: $CH_4/O_2 = 2/1$, total flow rate 300 $cm^3\ min^{-1}$; total pressure 0.1 MPa; catalyst weight 10 mg; contact time 2.0 ms.

catalyst bed during the CPO. In addition, in the CPO of methane without N_2 dilution, methane conversion was in the range of 76–78% for all catalysts tested except for Rh–CeO_2/MgO (Ce/Rh = 18.7) (71%), and it seems that the conversion was not influenced by the catalysts. This suggests that the effluent gas composition of the CPO without N_2 dilution almost reaches the equilibrium of steam reforming and water gas shift reactions within the experimental errors [19]. Fig. S4 shows the TEM image of Rh–CeO_2/MgO (Ce/Rh = 4) after the CPO of methane for 3 h. The catalytic performance was stable for 3 h and the TEM image indicates that the size of Rh metal particles was not changed (d_s = 3.8 ± 0.2 nm), and no deposited carbon such as whisker carbon was observed.

3.4. Oxidation degree during the CPO of methane

Table 5 lists out the results of the $CH_4 + O_2$ pulse reaction and subsequent titration of surface oxygen species. In the $CH_4 + O_2$ pulse reaction, the amount of CH_4 and O_2 was much larger than the adsorption amount of H_2 (number of surface atoms) as listed out in Table 1. The pulse of $CH_4 + O_2$ was supplied 10 times and the activity was not changed from the initial, and Table 1 lists out the stable activity. The order of methane conversion was as follows: Rh–CeO_2/MgO (Ce/Rh = 4) > Rh/MgO > Rh–CeO_2/MgO (Ce/Rh = 18.7). This activity order is similar to that of the CPO of methane with N_2 dilution as shown in Table 1. After the pulse reactions, we measured the amount of adsorbed and absorbed oxygen by the reaction of H_2 ($O(a) + H_2 \rightarrow H_2O$) at 1123 K. Generally, it is difficult to quench the catalyst under the steady-state conditions at high temperature without change in the surface state of the catalyst during ignition/extinction in the CPO of methane. Therefore, although the present results on the estimation of the degree of oxidation are qualitative, they are thought to be sufficiently suggestive. Methane-derived carbon-containing surface species such as CH_x and surface carbide have very low coverage due to much higher reactivity than that of methane. At the same time, the coverage of adsorbed hydrogen atom and CO can be very low due to high reaction temperature where the recombination of hydrogen atoms to H_2 molecule and the desorption of H_2 and CO are very favorable. Adsorbed oxygen atom can give considerable coverage since the dissociative adsorption of O_2 molecule is a fast elementary step. Therefore, the coverage of the reaction intermediates except for oxygen atom is so small that it may be possible to quench the surface state during the steady-state and pulse reactions. The order of the H_2 consumption amount was as follows: Rh/MgO > Rh–CeO_2/MgO (Ce/Rh = 18.7) > Rh–CeO_2/MgO (Ce/Rh = 4), and this also means the order of oxidation degree during the CPO of methane (Table 5). An important point is that the CeO_2 addition at the optimum amount can maintain the reduced state of catalysts during the reaction. The surface state of the catalysts can be strongly influenced by methane activation ability in the CPO of methane [28].

In addition, the H_2 adsorption on the Rh–CeO_2/MgO (Ce/Rh = 4) after the reaction was measured by using the present pulse technique, where the sample temperature was decreased to room temperature. The amount of H_2 consumption at the room temperature was 4.6 μmol g_{cat}^{-1} and this was close to the H_2 adsorption of the fresh Rh–CeO_2/MgO (Ce/Rh = 4) (Table 1). This suggests no drastic structural and morphological change during the reaction.

3.5. Ability to activate CH_4 of the catalysts

High methane activation ability is needed in order to maintain the reduced state even in the initial oxidation zone. Therefore, the ability to activate methane of the catalyst with the reduced and partially oxidized surface was evaluated using the pulse technique. Table 6 lists out the result of CH_4 pulse reaction on reduced and O_2-preadsorbed catalysts. It should be noted that the amount of methane feeding was less than or comparable to the number of Rh surface atom determined by the H_2 adsorption. On the reduced catalysts, the order of the methane reactivity was as follows: Rh–MgO > Rh–CeO_2/MgO (Ce/Rh = 4) > Rh–CeO_2/MgO (Ce/Rh = 18.7). On the other hand, since CeO_2/MgO has no reactivity of CH_4, the reactivity of methane normalized by surface Rh atoms is considered. The probability of activation, which is calculated by (the amount of reacted CH_4)/(the amount of surface Rh atoms) was estimated to be 0.36, 0.63, and 0.73 over Rh/MgO and Rh–

Table 5
H_2 titration after $CH_4 + O_2$ reaction over Rh/MgO and Rh–CeO_2/MgO (Ce/Rh = 4 and 18.7).

Catalyst	Number of surface Rh atoms (μmol)[a]	Pulse $CH_4 + O_2$ reaction[b] (4.0/2.0 μmol)			H_2 titration[c]	
		CH_4 conversion (%)	H_2 selectivity (%)	CO selectivity (%)	H_2 consumption (μmol)	Rh-based oxidation degree (%)[d]
Rh/MgO	0.22	78	74	69	0.48	34.4
Rh–CeO_2/MgO (Ce/Rh = 4)	0.12	85	77	71	0.05	3.6
Rh–CeO_2/MgO (Ce/Rh = 18.7)	0.08	54	35	63	0.25	17.9

[a] H_2 adsorption.
[b] CH_4/O_2 reaction conditions: CH_4/O_2 = 4.0/2.0 μmol (300 $cm^3\ min^{-1}$ He carrier; 2.0 ms); T_{TC} = 873 K; total pressure 0.1 MPa; catalyst weight 10 mg (0.93 μmol-Rh).
[c] H_2 = 0.46 μmol (100 $cm^3\ min^{-1}$ He carrier at 1123 K).
[d] (H_2 consumption [μmol])/(1.5 × (Rh amount [μmol])) × 100.

Table 6
Results of the pulse reaction of methane on reduced and O_2-preadsorbed catalysts.

Catalyst	Amount (μmol)			Amount of preadsorbed oxygen atom (μmol)	CH_4 pulse reaction (μmol)[a]	
	Rh	CeO_2	Surface Rh[b]		Reacted CH_4	Formed H_2
Rh/MgO	9.3	0	2.2	0	0.79	0.71
				4.6	0.81	0.20
Rh–CeO_2/MgO (Ce/Rh = 4)	9.3	37	1.2	0	0.76	0.61
				4.8	0.84	0.65
Rh–CeO_2/MgO (Ce/Rh = 18.7)	9.3	174	0.8	0	0.58	0.51
				4.8	0.67	0.48
6.4 wt% CeO_2/MgO[c]	–	37	–	0	0	0
				4.8	0	0

[a] Reaction conditions: CH_4 = 1.2 μmol (100 cm^3 min^{-1} He carrier); T_{TC} = 773 K; total pressure 0.1 MPa; catalyst weight 100 mg (9.3 μmol-Rh).
[b] H_2 adsorption.
[c] Loading amount of CeO_2 on 6.4 wt% CeO_2/MgO was equal to that on Rh–CeO_2/MgO (Ce/Rh = 4).

CeO_2/MgO (Ce/Rh = 4 and 18.7). The results indicate that the addition of CeO_2 enhanced the probability of methane activation. In the reaction, hydrogen was formed as a product and the selectivity to hydrogen was similar among the catalysts. Carbon-containing products such as CO and CO_2 were not observed at all, and this represents that carbon-containing surface species such as CH_x and surface carbide can be present on the catalyst surface. In this case, the amount of carbon-containing species was smaller than the number of the surface Rh atoms, and the formation of solid carbon such as whisker carbon is not expected. When the catalysts were treated with oxygen pulses up to O/Rh = 0.5, the reactivity of CH_4 on Rh/MgO was almost unchanged, but the H_2 formation was strongly suppressed. The Rh/MgO with preadsorbed oxygen can also activate methane to give H_2O, which cannot be detected by our experimental system. In contrast, on Rh–CeO_2/MgO (Ce/Rh = 4 and 18.7), the reactivity of methane increased slightly by preadsorption of oxygen and the amount of H_2 formation was almost maintained. This behavior suggests that the preadsorbed oxygen is adsorbed on reduced Ce species, and metallic Rh surface is maintained. At the same time, partial dewetting of Ce species by the oxidation [35] can increase the number of surface Rh metal atom; this can enhance the amount of reacted methane and formed H_2. The role of added CeO_2 on Rh–CeO_2/MgO has two aspects. One is to prevent the oxidation of Rh with O_2 as mentioned above. The other is the enhancement of methane activation rate per the Rh surface site. Based on the characterization results, the surface of Rh metal particles is partially covered with the reduced CeO_2 species, indicating that Rh–CeO_2/MgO catalysts have large interface between Rh and Ce species, and it is suggested that the role of the interface on the methane activation can be due to oxide ions present in the interface. It has been reported that the activation of methane on metal surfaces can be promoted by the adsorbed oxygen atom to give methoxy and hydroformyl species according to the previous reports [49–51].

3.6. Interpretation of temperature profiles in the catalytic partial oxidation of methane

Based on the previous reports, the CPO of methane has two reaction zones: the initial oxidation of methane to CO and CO_2, and the stream reforming of residual methane at downstream [44,45]. In the initial oxidation zones, O_2 is present in the gas phase, and the catalysts tend to be oxidized. The obtained oxidation degree of catalysts by H_2 titration after the pulse CPO (Table 5) is associated with the initial oxidation zone. The results given in Table 5 show that the degree of oxidation is strongly dependent on the catalysts and that Rh/MgO was more deeply oxidized than Rh–CeO_2/MgO (Ce/Rh = 4). This behavior does not agree with the previous results that the O_2 consumption rate is typically controlled by the mass transfer and the length of oxidation zone is almost unchanged [19,52]. Much different degree of oxidation suggests that the length of oxidation zone may be changed. Further investigation is necessary regarding the mass transfer limitation of O_2 in the present catalytic systems.

The steam reforming of methane is a main reaction at downstream, and the metallic surface has the catalytic activity of steam reforming of methane. The activity of steam reforming of methane was evaluated on the reduced Rh/MgO and Rh–CeO_2/MgO (Ce/Rh = 4), and the results are listed out in Table S1. The CH_4 conversion in methane steam reforming on Rh–CeO_2/MgO (Ce/Rh = 4) was a little lower than that on Rh/MgO. This behavior almost agreed with the ability to activate methane of the catalysts without preadsorbed oxygen (Table 6). On the other hand, high steam reforming activity on the reduced Rh/MgO than that on the reduced Rh–CeO_2/MgO (Ce/Rh = 4) cannot explain the results of the CPO with or without N_2 dilution.

In the case of the CPO with N_2 dilution (Table 1), methane conversion on Rh/MgO was lower than that on Rh–CeO_2/MgO (Ce/Rh = 4). This tendency is interpreted to be due to Rh/MgO with deeper oxidation, which can decrease the amount of reduced and active surface for steam reforming. In contrast, the oxidation of Rh–CeO_2/MgO (Ce/Rh = 4) is suppressed and the amount of reduced and active surface is maintained, although Rh–CeO_2/MgO (Ce/Rh = 4) was not so active for steam reforming as Rh/MgO in the fully reduced state.

In the case of the CPO without N_2 dilution, Rh–CeO_2/MgO (Ce/Rh = 4) showed lower catalyst bed temperature than Rh/MgO (Fig. 3). The highest bed temperature can be determined by the exothermic reaction in the oxidation zone and the effect of the overlap with the endothermic steam reforming zone [19,46–48]. In the case of Rh–CeO_2/MgO (Ce/Rh = 4), the formation of the oxidized surface can be suppressed as expected from the results of the CPO with N_2 dilution (Tables 1 and 5). This enables larger overlap of the oxidation reaction zone with the reforming zone since the reforming reaction can proceed on the reduced metallic surface. In addition, Rh metal particles partially covered with reduced Ce species on the reduced Rh–CeO_2/MgO are suggested by characterization results. In contrast, it has been reported that this decoration of Rh particles with Ce species is reversible under O_2-containing atmosphere [35]. Therefore, the available Rh surface atoms on Rh–CeO_2/MgO under the CPO may be larger than those on the reduced Rh–CeO_2/MgO. In fact, this phenomenon can explain the increase of the reacted CH_4 amount by O_2 preadsorption on Rh–CeO_2/MgO (Ce/Rh = 4) in Table 6. In this experiment, the Rh-based oxidation degree is calculated as 0.34. On the other hand, the oxidation degree of Rh–CeO_2/MgO (Ce/Rh = 4) determined in Table 5 is 0.036 and it was much smaller. Judging from the small oxidation degree of Rh–CeO_2/MgO (Ce/Rh = 4), the increase of the available Rh surface atoms by dewetting of Ce species is not a main reason for the effect of CeO_2 addition in the CPO of methane.

In the CPO of methane, water gas shift (WGS) reaction ($CO + H_2O \rightarrow CO_2 + H_2$, $\Delta H = -41$ kJ/mol) proceeds as well as the oxidation of methane and the steam reforming of methane. Since the heat due to the WGS is much smaller than those due to the methane oxidation and steam reforming, it is difficult to recognize the reaction zone by our experimental setup. Based on the outlet temperature and the composition of the effluent gas in the CPO of methane without N_2 dilution (Table 4), we calculate the equation below [19]:

$$\left(\frac{K_{EXP}}{K_{EQ}}\right)_{WGS} = \frac{P_{H_2}P_{CO_2}}{P_{CO}P_{H_2O}} \cdot \frac{1}{K_{EQ,WGS}}$$

Here, K_{EQ} is the equilibrium constant calculated with the outlet temperature, and P_i are the partial pressures of species i. The values of Rh/MgO and Rh–CeO_2/MgO (Ce/Rh = 4) are 2.4 and 2.8, respectively. The difference is so small that it is difficult to discuss the effect of CeO_2 on the equilibrium approach of the WGS reaction.

On the other hand, Rh–CeO_2/MgO (Ce/Rh = 18.7) showed low methane conversion in the CPO of methane with N_2 dilution and high bed temperature in the CPO without dilution. As shown in Table 6, the ability to activate methane of Rh–CeO_2/MgO (Ce/Rh = 18.7) was inferior to Rh/MgO and Rh–CeO_2/MgO (Ce/Rh = 4), although the small increase of reacted methane amount that could be interpreted by dewetting effect of Ce oxidation was observed. Low ability to activate methane is related to high oxidation degree in the CPO of methane as listed out in Table 5. Both low steam reforming activity and high oxidation degree during the CPO bring about the bed temperature increase in the CPO without N_2 dilution and the decrease of methane conversion in the CPO with N_2 dilution on Rh–CeO_2/MgO (Ce/Rh = 18.7).

4. Conclusions

The additive amount of CeO_2 over Rh–CeO_2/MgO was optimized at Ce/Rh = 4 in terms of highest methane conversion in the catalytic partial oxidation (CPO) of methane with N_2 dilution and lowest catalyst bed temperature in the CPO of methane without N_2 dilution. Characterization results indicated that the addition of CeO_2 to Rh/MgO decreased Rh metal particle size monotonously with increasing CeO_2 amount, and that Rh metal particles were partially covered with the Ce species on Rh–CeO_2/MgO catalysts. As a result of the pulse CPO of methane, the optimized Rh–CeO_2/MgO (Ce/Rh = 4) exhibited much lower oxidation degree of the catalysts than Rh/MgO and Rh–CeO_2/MgO (Ce/Rh = 18.7). High resistance to oxidation of Rh–CeO_2/MgO (Ce/Rh = 4) can be caused by high ability to activate methane, on the reduced catalyst and even on the catalyst with preadsorbed oxygen. The catalyst bed of the CPO of methane mainly consists of the oxidation and the steam reforming zones. High resistance to oxidation of Rh caused by the presence of CeO_2 is thought to decrease the ratio of the oxidized catalysts and to increase simultaneously the ratio of the catalysts with the reduced surface. High methane conversion in the CPO of methane over Rh–CeO_2/MgO (Ce/Rh = 4) with N_2 dilution can be due to higher ratio of the reduced catalyst. At the same time, the decrease in the catalyst bed temperature in the CPO of methane without N_2 dilution on the Rh–CeO_2/MgO (Ce/Rh = 4) with higher resistance to the oxidation of Rh can be due to the promotion of the overlap between the exothermic oxidation reaction zone and the endothermic reforming zone.

Acknowledgments

We sincerely thank Japan Oil, Gas and Metals National Corporation (JOGMEC) and Chiyoda Corporation for financial support.

Appendix A. Supplementary data

Supplementary data associated with this article can be found, in the online version, at doi:10.1016/j.jcat.2009.08.008.

References

[1] J.R. Rostrup-Nielsen, J. Sehested, J.K. Nørskov, Adv. Catal. 47 (2002) 65.
[2] J.R. Rostrup-Nielsen, Catal. Today 145 (2009) 72.
[3] D.A. Hickman, L.D. Schmidt, J. Catal. 138 (1992) 267.
[4] D.A. Hickman, L.D. Schmidt, Science 259 (1993) 343.
[5] R. Horn, K.A. Williams, N.J. Degenstein, A. Bitsch-Larsen, D. Dalle Nogare, S.A. Tupy, L.D. Schmidt, J. Catal. 249 (2007) 380.
[6] C. Elmasides, T. Ioannides, X.E. Verykios, ALChE J. 46 (2000) 1260.
[7] B.C. Enger, R. Lødeng, A. Holmen, Appl. Catal. A 346 (2008) 1.
[8] H.C. Yao, Y.F. Yu Yao, J. Catal. 86 (1984) 254.
[9] N.R. Collins, M.V. Twigg, Top. Catal. 42–43 (2007) 323.
[10] A. Gayen, K.R. Priolkar, P.R. Sarode, V. Jayaram, M.S. Hedge, G.N. Subbanna, S. Emura, Chem. Mater. 16 (2004) 2317.
[11] K. Nagaoka, K. Sato, S. Fukuda, S. Nakashiki, H. Nishiguchi, J.A. Lercher, Y. Takita, Chem. Mater. 20 (2008) 4176.
[12] R. Wang, H. Xu, X. Liu, Q. Ge, W. Li, Appl. Catal. A 305 (2006) 204.
[13] M. Asadullah, S. Ito, K. Kunimori, M. Yamada, K. Tomishige, J. Catal. 208 (2002) 255.
[14] T. Miyazawa, K. Okumura, K. Kunimori, K. Tomishige, J. Phys. Chem. C 112 (2008) 2574.
[15] P.J. Dauenhauer, B.J. Dreyer, N.J. Degenstein, L.D. Schmidt, Angew. Chem., Int. Ed. 46 (2007) 5864.
[16] J.R. Salge, G.A. Deluga, L.D. Schmidt, J. Catal. 235 (2005) 69.
[17] W. Cai, F. Wang, A.C. Van Veen, H. Provendir, C. Mirodatos, W. Shen, Catal. Today 138 (2008) 152.
[18] I. Cuautémoc, G.D. Angel, G. Torres, V. Bertin, Catal. Today 133–135 (2008) 588.
[19] A. Donazzi, B.C. Michael, L.D. Schmidt, J. Catal. 260 (2008) 270.
[20] B.C. Micael, A. Donazzi, L.D. Schmidt, J. Catal. 265 (2009) 117.
[21] A. Bitsch-Larsen, N.J. Degenestein, L.D. Schmidt, Appl. Catal. B 78 (2008) 364.
[22] K. Tomishige, Y.G. Chen, K. Fujimoto, J. Catal. 181 (1999) 91.
[23] Y.G. Chen, K. Tomishige, K. Yokoyama, K. Fujimoto, Appl. Catal. A 165 (1997) 335.
[24] K. Imagawa, A. Nagumo, R. Kanai, T. Minami, K. Tomishige, Y. Suehiro, Stud. Surf. Sci. Catal. 167 (2007) 415.
[25] H.Y. Wang, E. Ruckenstein, J. Catal. 186 (1999) 181.
[26] E. Ruckenstein, H.Y. Wang, J. Catal. 190 (2000) 32.
[27] E. Ruckenstein, H.Y. Wang, Appl. Catal. A 198 (2000) 33.
[28] S. Naito, H. Tanaka, S. Kado, T. Miyao, S. Naito, K. Okumura, K. Kunimori, K. Tomsihge, J. Catal. 259 (2008) 138.
[29] J.R. Anderson, Structure of Metallic Catalysts, Academic Press, New York, 1975. p. 358.
[30] D.G. Mustard, C.H. Bartholomew, J. Catal. 67 (1981) 186.
[31] N. Seshu Babu, N. Lingaiah, R. Gopinath, P. Siva Sankar Reddy, P.S. Sai Prasad, J. Phys. Chem. C 111 (2007) 6447.
[32] B. Li, S. Kado, Y. Mukainakano, T. Miyazawa, T. Miyao, S. Naito, K. Okumura, K. Kunimori, K. Tomishige, J. Catal. 245 (2007) 144.
[33] Y. Mukainakano, B. Li, S. Kado, T. Miyazawa, K. Okumura, T. Miyao, S. Naito, K. Kunimori, K. Tomishige, Appl. Catal. A 318 (2007) 252.
[34] J.R. Anderson, Structure of Metallic Catalysts, Academic Press, New York, 1975. p. 289.
[35] S. Bernal, F.J. Bontana, J.J. Calvino, G.A. Cifredo, J.A. Pérez-Omil, J.M. Pintado, Catal. Today 23 (1995) 219.
[36] C. Force, J.P. Belzunegui, J. Sanz, A. Martínez-Arias, J. Soria, J. Catal. 197 (2001) 192.
[37] J. Stubenrauch, J.M. Vohs, Catal. Lett. 47 (1997) 21.
[38] K. Tomishige, A. Okabe, K. Fujimoto, Appl. Catal. A 194–195 (2000) 383.
[39] R. Ueda, T. Kusakari, K. Tomishige, K. Fujimoto, J. Catal. 194 (2000) 14.
[40] G.L. Haller, D.E. Resasco, Adv. Catal., vol. 36, Academic Press, New York, 1989. p. 173.
[41] S.J. Tauster, Acc. Chem. Res. 20 (1987) 389.
[42] R. Horn, N.J. Degenstein, K.A. Williams, L.D. Schmidt, Catal. Lett. 110 (2006) 169.
[43] R. Horn, K.A. Williams, N.J. Degenstein, L.D. Schmidt, J. Catal. 242 (2006) 92.
[44] T. Liu, C. Snyder, G. Veser, Ind. Eng. Chem. Res. 46 (2007) 9045.
[45] D.D. Nogare, N.J. Degenstein, R. Horn, P. Canu, L.D. Schmidt, J. Catal. 258 (2008) 131.
[46] K. Tomsihgie, S. Kanazawa, K. Suzuki, M. Asadullah, M. Sato, K. Ikushima, K. Kunimori, Appl. Catal. A 233 (2002) 35.
[47] B. Li, K. Maruyama, M. Nurunnabi, K. Kunimori, K. Tomishgie, Appl. Catal. A 275 (2004) 157.
[48] B. Li, S. Kado, Y. Mukainakano, M. Nurunnabi, T. Miyao, S. Naito, K. Kunimori, K. Tomishige, Appl. Catal. A 304 (2006) 62.
[49] T. Sasaki, K. Nakao, K. Tomishige, K. Kunimori, Appl. Catal. A 328 (2007) 140.
[50] T. Sasaki, K. Nakao, K. Tomishige, K. Kunimori, Chem. Commun. (2006) 3821.
[51] M.A. Quinlan, B.J. Wood, H. Wise, Chem. Phys. Lett. 118 (1985) 478.
[52] M. Maestri, A. Beretta, G. Groppi, E. Tronconi, P. Forzatti, Catal. Today 105 (2005) 709.